

Bio-synthesis and Photocatalytic Activity of Zinc Oxide Nanoparticles for Sulfosulfuron Herbicide Degradation from Aqueous Solutions

Israa Sabah Abass^{1,2*}, Abeer I Alwared¹

¹ Department of Environmental Engineering, College of Engineering, University of Baghdad, Iraq

² Ministry of Water Resources, Baghdad, Iraq

* Corresponding author's e-mail: israa.sabah2111p@coeng.uobaghdad.edu.iq

ABSTRACT

In this study, zinc oxide (ZnO) nanoparticle was fabricated using the extract of Olive leaves (referred as ZnO NPs), using the green synthesis process, and then explores its ability for photodegradation of different concentrations of sulfosulfuron herbicide (10, 20, 40, and 80) mg/L under visible light in batch mode system at pH of 6.8 and one g/L of ZnO NPs. Morphological and structural properties of the synthesized ZnO NPs have been characterized using X-ray diffraction (XRD), fourier transform infrared (FTIR), brunauer Emmett Teller (BET), vibrating sample-magnetometer (VSM), transmission electron microscope (TEM), scanning electron microscopy (SEM). The finding confirms that the maximum removal efficacy reached 82.08% under optimum conditions of 10 mg/L of sulfosulfuron Herbicide concentration, and 90 min. In addition, the reaction followed a first-order kinetics model with $R^2 > 96$. The study also showed that ZnO NPs could be used as a catalyst for four cycles of photocatalytic oxidation of organic contaminants before losing its effectiveness. According to the finding of this study, ZnO NPs has an acceptable efficiency in the elimination of herbicide, as their relatively simple synthesis, could be a suitable catalyst for the degradation and elimination of pharmaceutical residues.

Keywords: olive leaf extract, green synthesis, ZnO, photocatalytic, herbicide, kinetic study.

INTRODUCTION

Nanotechnology is one of the most quickly evolving fields, potentially forming and underpinning a wide range of technological and biotechnological advancements; as a result, it is seen as the century's oncoming industrial revolution (Bhardwaj et al., 2020). Nanotechnology has been used in different industrial and academic areas, including chemistry, agriculture, biology, medicine, electronics, information technology and physics (Patil and Kim, 2017; Dash et al., 2020). Nanomaterials possess great potential in various fields of science due to their excellent physico-chemical and biological characteristics over bulk materials (Al-Rbaiha et al., 2023). Nanoparticles (NPs) have the unique property of having a high surface-to-volume ratio (Sulaiman et al., 2022), which means that they are more appropriate candidates for application-oriented

performance (e.g., photocatalysis, cosmetics, gas sensing, energy reservoirs, electronics, packaging and environmental remediation) and encourages their incorporation into a wide range of commercial products, biotechnology and biomedical applications (Zheng et al., 2020). Among the large variety of NPs available, metal oxide (MO) NPs are thought to be the most promising because they have distinctive physical, chemical, and biological properties like solubility, chemical stability, and adhesiveness (Abdelbaky et al., 2022).

ZnO nanomaterials have been the most widely utilized n-type semiconductor ingredient having a wide band gap (3.37 eV) and large excitation energy. ZnO is a low-cost, non-toxic, chemically resistant material having wide variety of applications in sensors, solar devices, drug delivery, catalysis, etc (Patwa et al., 2021). There are several physical and chemical techniques for creating ZnO nanoparticles, yet none of them are

practicable from an environmental or commercial standpoint for use in industry. As a result, the utilization of organic, natural materials for functionalization, stabilizers, and templates is becoming more common. Industrial wastewaters, such as dyes and organic compounds, can be treated by photocatalysis, an effective and non-toxic method that produces highly reactive hydroxyl radicals (Patwa et al., 2021).

A massive list of properties used in the biological synthesis of metal nanoparticles exists. Plant parts, algae, fungus, bacteria, and viruses are used in the biological synthesis of nanoparticles (Hamouda et al., 2021). Herbal cuttings arranged from leaf, stalks, origins, floras, and pips of plants, because of differences in composites, have unlikely possessions on the quantity and physiognomies of created nanoparticles (Raafat et al., 2021). Shrubberies have a great deal of ordinary reformative and steadying materials. Plants are broadly dispersed and simply available, and they are sources of various metabolites (Asemani et al., 2019). Actual phytochemicals in the manufacture of nanoparticles contain terpenes, flavonoids, ketones, aldehydes, and carboxylic acid (Ahmad et al., 2019). Additionally, reducing agents like protein, enzymes, and others have a vital role in metallic nanoparticle creation by green plants (Abbasian et al., 2020). The biosynthesis techniques grow nanoparticles of good surface morphology and clear size as related to some of other physicochemical synthesization techniques (Sarli et al., 2020). The biological growth of nanoparticles depends on the existence of enzymes as well as proteins included in their depositions. Nanoscience has numerous advantages in smart medicinal providing systems (Abel et al., 2021).

Due to their long-term persistence in soil, high water solubility, and photochemical stability, contamination of water resources with pesticides used in agriculture is a cause for environmental concern (Pergal et al., 2018).

Organic contaminants like pesticides are commonly found in industrial wastewater sources, urban areas, and agricultural regions. Pesticides present in water and wastewater pose a hazard to the environment and are very toxic, which has led to an increase in public health issues (Mohammed et al., 2024)

Sulfonylureas are a large family of herbicides widely used for control of broad leaf weeds in various crops and vegetables as well as industrial weeds. They have gained attention more so than other pesticides due to their good crop selectivity, low application rates, and favorable

environmental properties. However, due to their high solubility in water, moderate to high mobility, and slow degradation, they are now being detected in surface and ground waters. Moreover, they express low to acute mammalian toxicity. Therefore, effective, low cost, and robust methods to decontaminate waters are needed, as long as they do not further stress the environment or endanger human health (Paporisch et al., 2020).

Some of these herbicides are known to be highly persistent in the soil, with a long-term residual activity that results in damage to sensitive plants for up to several years after application to the soil for selective weed management (Prasad et al., 2018). Conventional water treatments cannot completely remove pesticides, for example, adsorption and bioremediation. Their removal from the environment, especially from surface waters, is now an imperative and is the subject of studies which have involved numerous researchers for several years now.

As an alternative approach to conventional wastewater treatment, advanced oxidation processes, such as heterogeneous photocatalysis, have been extensively studied because of their high potential in the degradation of pesticides (Navarraa et al., 2023). Generally, photocatalysis involves using a semiconductor material as well as a source of radiation (UV, sunlight, and visible light) to produce free radicals. When photons collide with the catalyst surface, electrons are excited and move from the phases of the gap to band conductors while also creating cavities (holes) at the catalyst surface. At last, the reactive radical hydroxyl (OH) will be produced when these holes interact with water molecules or OH ions (Alward et al., 2023).

In this study, the green synthesis of ZnO nanoparticles using the extract of olive was performed by employing the citrate combustion method. Then after it was used for the first time in the photodegradation of sulfosulfuron herbicide found in water-based solutions. Using the (XRD, FTIR, BET, VSM, TEM, SEM, PL, DRS, EDS, and elemental mapping) analyses, structural properties in the photocatalyst were ascertained.

MATERIALS AND METHODS

Materials

All used chemicals were purchased from Thomas Baker, India, and utilized without further purification. zinc nitrate $Zn(NO_3)_2$ with 98% purity,

deionized water. $\text{NH}_4\cdot\text{H}_2\text{O}$ aqueous and grade sulfosulfuron herbicide (98.8 % purity) was selected as a contaminated sample. In addition, 0.1 M of sodium hydroxide and/or hydrochloric acid (HCl) were employed to neutralize and regulate the pH.

Preparation of olive leaves extracts

The fresh olive leaves (*Olea europaea*) were collected, cleaned thoroughly in tap water, and then rinsed with distilled water. They were then boiled for two hours at 70 degrees Celsius in 125 mL of distilled water. After that, the extracted solution was filtered and put away for later use (Abdulrazaq and Alward, 2023).

Biosynthesis of zinc oxide nanoparticles

Bio synthesis of ZnO NPs was conducted according to the methods cited in (Hashemi et al.,

2016) with some modifications, the method was as follows: 20 mL of olive leaves extract were mixed with 80 mL of deionized water then heated at 60 °C using a stirrer heater. Then, 5 grams of zinc nitrate mixed with $\text{NH}_4\cdot\text{H}_2\text{O}$ extracts and stirred at pH 10 at 80° for 1 hour with speed of 400 rpm for stirrer. The dough was obtained at 80 °C after 1 h heating the mixture. The dough was annealed and dried in furnace at 400 °C for 2 h. After heating, the material was powdered by mortar and pestle. Then powder was centrifuged three times at 10000 rpm for 30 min and supernatant was discarded. Then after keeping the powder for later use (Figure 1A). The flowchart for research methodology was shown in (Figure 1B)

Photocatalytic activity

The photodegradation performance of the generated catalysts against sulfosulfuron herbicide

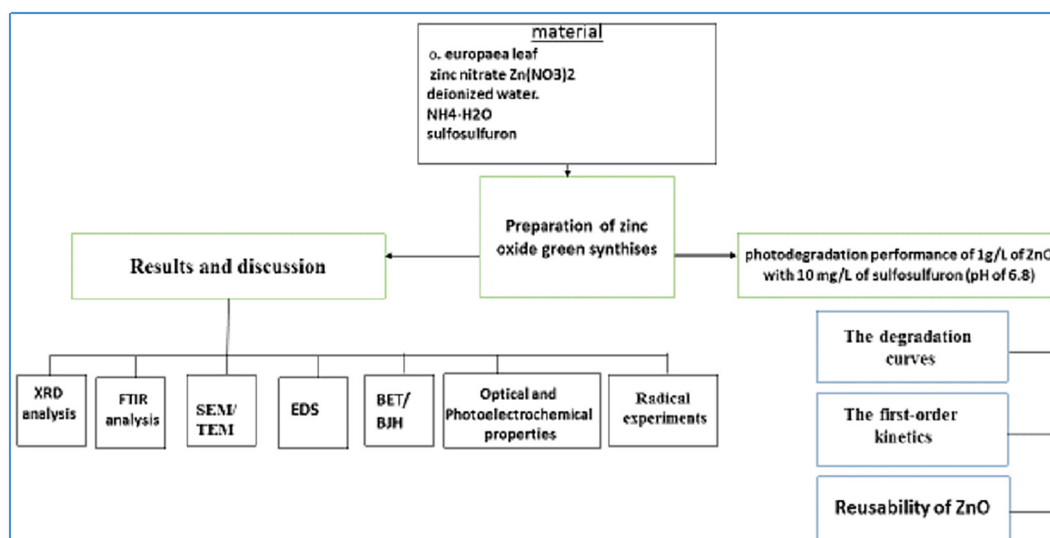
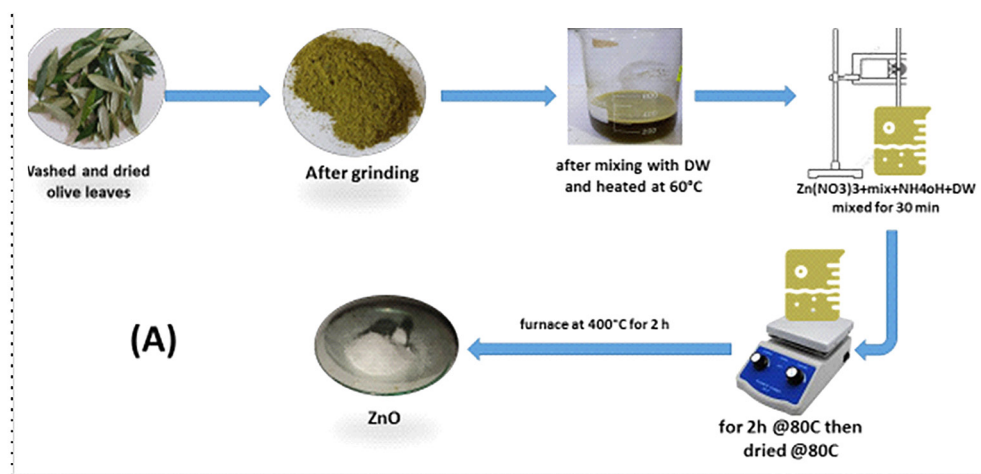


Figure 1. Schematic illustration for (A) ZnO fabrication, (B) Research methodology flowchart

has been studied using a batch reactor. To put it briefly, 100 mL of sulfosulfuron solution had been combined with 100 mg of photocatalyst at a concentration of 10 mg/L. Agitating the mixture for thirty minutes in the dark control reactor, allowed investigator to examine the synthesized photocatalyst's adsorption performance. Following the state of equilibrium between adsorption and desorption, the reactor was exposed to two LED lamps, each with a power of 50 W and a light intensity of $39.8 \text{ mW}\cdot\text{cm}^{-2}$, while being stirred for a duration of 90 minutes. Ten centimeters was applied as to separate between the illumination source and reactor. A 3 mL sample of sulfosulfuron was taken out of the reactor every 15 minutes, and the ultimate concentration of sulfosulfuron was measured at 212 nm using a UV-vis spectrophotometer (UV1200-Spectrophotometer, China). Equation 1

was utilized to determine the photodegradation efficiency of the produced photocatalyst against sulfosulfuron (Mohammed et al., 2020).

$$DP(\%) = \frac{C_o - C_t}{C_o} \times 100 \quad (1)$$

where: DP represents photodegradation performance (%), C_o represents the initial sulfosulfuron concentration (mg/L), C_t represents the treated sulfosulfuron concentration at time (t)

RESULTS AND DISCUSSION

The chemical structure

As seen in (Figure 2A), the goal of the XRD analysis was to look at the crystalline phase of the

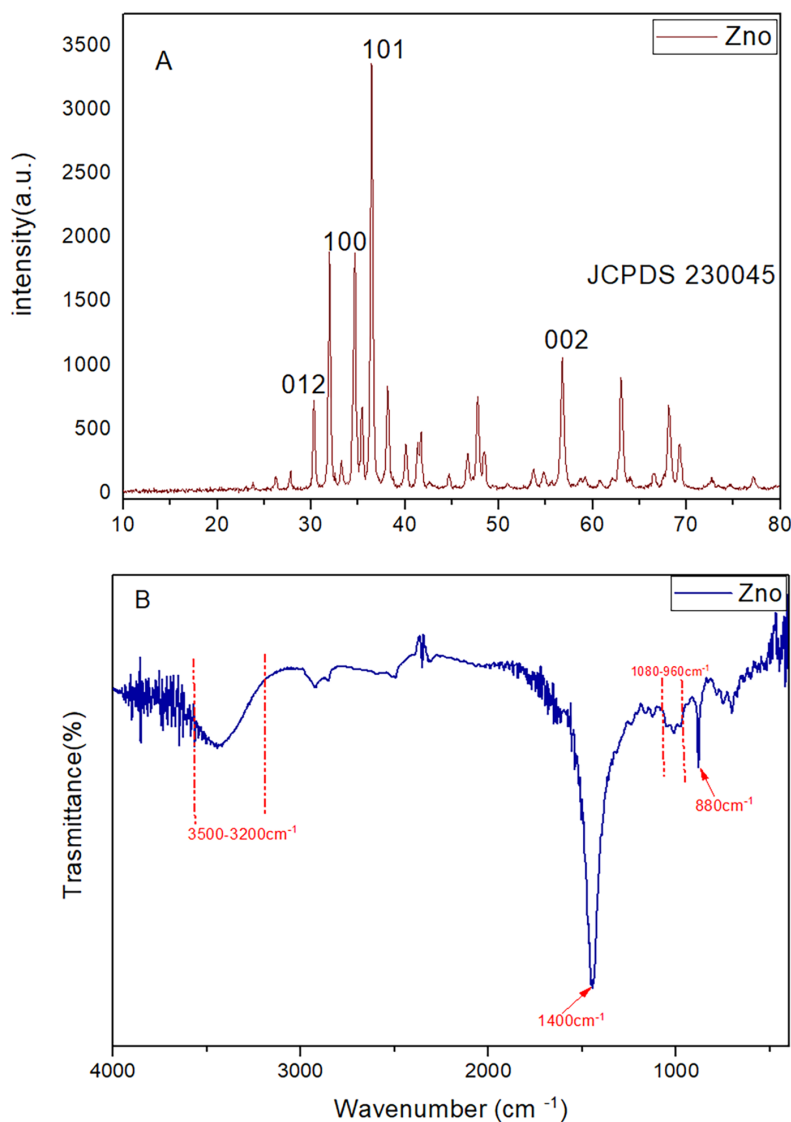


Figure 2. The structure characterization of ZnO, (A) XRD patterns, (B) FTIR spectra

produced samples (ZnO). The narrow and acute diffraction peaks appear at 30.22° , 32.04° , 36.37° , 47.82° , and 56.63° appear at about 2θ . Corresponding results have also been documented (Schreyer et al., 2014). It has also been shown that these diffraction peaks expand, which can be attributed to moderately crystallinity and small nanoscale particle sizes. For the XRD investigation, the dry powders of the zinc nanoparticles were utilized. From 10° to 80° , the diffracted intensity was measured at 2θ angles and measured. Similar X-ray diffraction patterns were also obtained by previous research for the green synthesis of zinc oxide nanoparticles; metallic zinc oxide is verified in ZnO NPs that are biosynthesized (Alrubaie et al., 2019).

To find out more about the chemical structure of the produced photocatalyst, FTIR spectroscopy was used, and their results are introduced in (Figure 2B). As can be seen in this figure that the FTIR spectra of zinc nanoparticles is clearly visible with absorption peaks ranges between 400 and 4000 cm^{-1} . Bands found at $(3500\text{--}3200)\text{ cm}^{-1}$ are attributed to the O-H phenol group vibrations stretching. It is possible to attribute the bands observed at 2918.656 cm^{-1} to the stretching C-H alkaline vibrations. The bands $(1485.07, 1369.4)\text{ cm}^{-1}$ may correspond to an aromatic ring's C-C stretching. The bands observed at 1080 cm^{-1} may correspond to amine stretching. This outcome is comparable to the previously published findings of the production of ZnO nanoparticles utilizing *Acalypha indica* leaf extract (Gnanasangeetha et al., 2013). Protein vibrations that stretch Si-O-Si could be attributed to the bands seen at 1016.49 cm^{-1} . The C-N stretching amine may be assigned to the band at (695.5 cm^{-1}) , and the bands may be allotted to the secondary amine wagging at 960 cm^{-1} . The bands' change to a much lower frequency provides

evidence of these chemicals' deposition during the creation of ZnO NPs. This result is consistent with previously published findings on the production of ZnO nanoparticles utilizing extract from olive leaves (Awwad et al., 2014). The existence of phenolic compounds and proteins was assured by the functional vibrations bands group as demonstrated in the FTIR spectrum.

Surface morphologies

The SEM image of a ZnO NPs the size and the morphology of the biosynthesized ZnO nanoparticles were imaged SEM (Figure 3A), the SEM image demonstrated that the ZnO NPs were spherical and hexagonal in the morphology shape with good distribution, with an average size of ZnO NPs of 29.03 nm. The high-resolution TEM analysis (Figure 3B) was carried out to confirm the formation of the biosynthesized ZnO NPs. Based on the results obtained, it can be concluded that the pure green ZnO NPs display hexagonal and also clearly reveal lattice fringes without any distortion, indicating that ZnO NPs have high crystallinity, indicating that ZnO nanoparticles are crystalline in nature (Andrade et al., 2024). The chemical composition of the biosynthesized ZnO nanoparticles was determined using EDS (Figure 4). The elemental mapping of the EDS verified that the examined sample displayed the elemental peaks of zinc and oxygen, which confirms the existence of ZnO NPs (Abdelbaky et al., 2022).

Additionally, the hexagonal wurtzite crystalline structure of ZnO NPs is also proven by the diffraction rings on the peaks in the XRD pattern. Finally, the surface properties of Zinc oxide nano particle were performed using the N_2

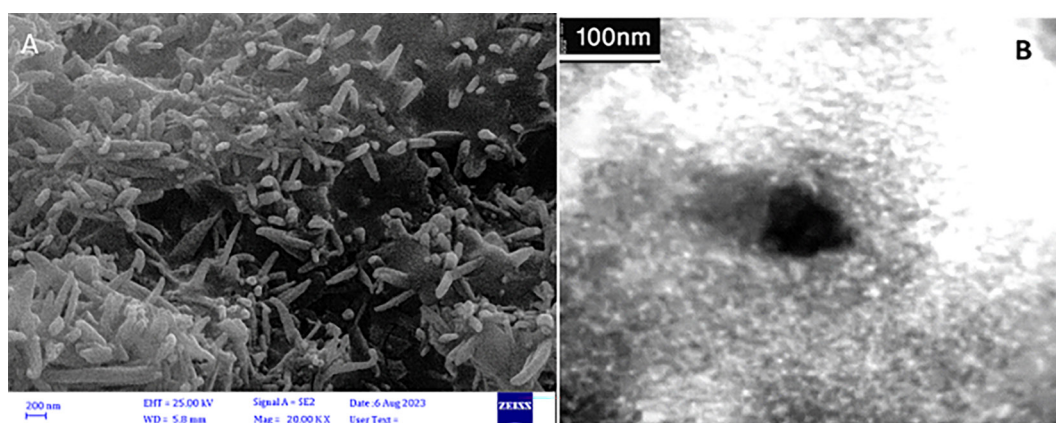


Figure 3. SEM images of (A) ZnO nanoparticle (B) TEM image of ZnO

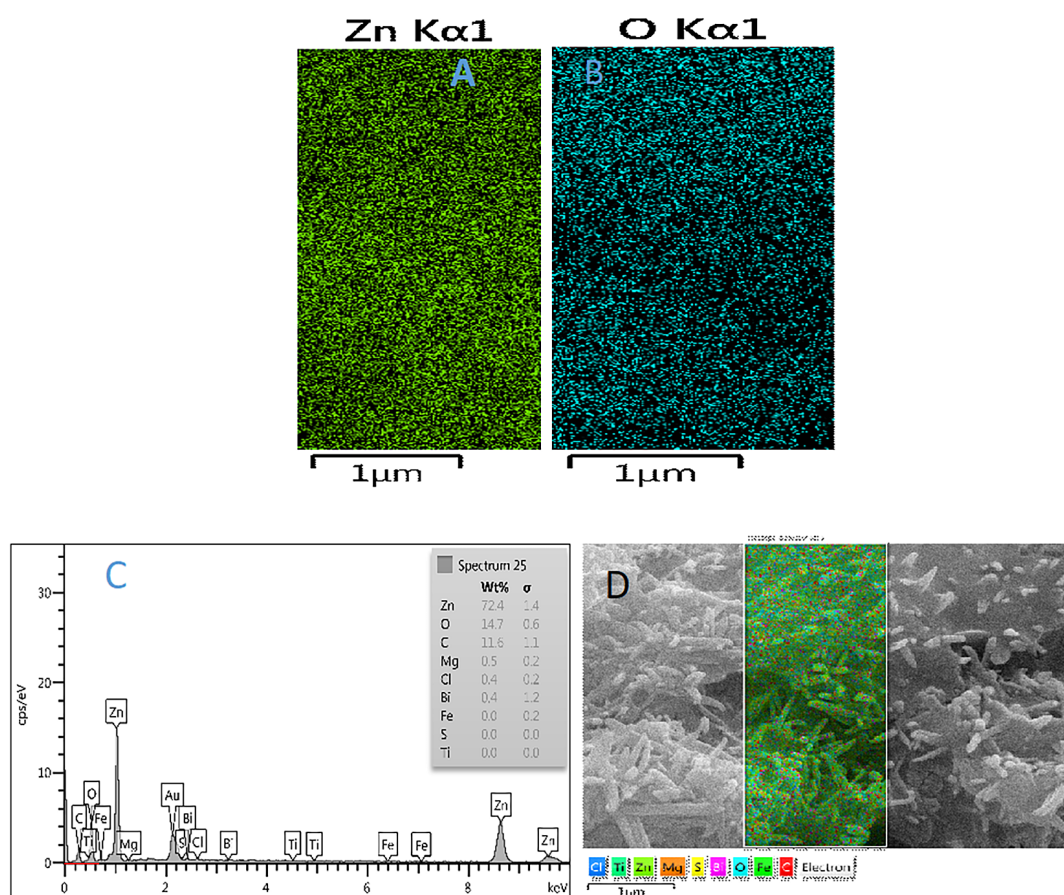


Figure 4. EDS analysis (A and B) elemental mapping of Zn, and O elements, (C and D) EDS spectrum

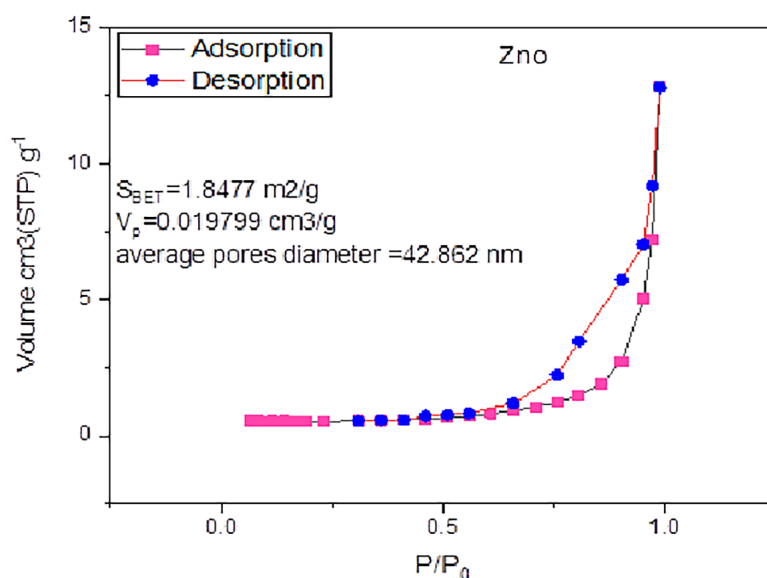


Figure 5. N_2 adsorption-desorption curves of ZnO NPs

adsorption-desorption isotherm (Figure 5). the specific surface area (S_{BET}), total pore volume (V_p), and average pores diameter were revealed to be 1.8477 m^2/g , 0.019799 cm^3/g , and 42.862 nm.

Optical and photoelectrochemical properties

The DRS technique was performed to analyze the optical property of ZnO nanoparticle,

and their results were shown in (Figure 6A). The UV-vis spectrometer was used to study the absorbance spectra of ZnO NPs in the wavelength range between 200–800 nm. The optical band gap energy (E_g) of the samples is determined by fitting the absorption data using Tauc Equation 2.

$$(\alpha h\nu)^{1/n} = A (h\nu - E_g) \quad (2)$$

where: $h\nu$ is the photon energy, E_g is the direct band gap, and A is a constant. α is the optical absorption coefficient and found from the absorption data.

The optical band gap of the prepared ZnO NPs was obtained by plotting $(\alpha h\nu)^2$ as a function of photon energy ($h\nu$), (Figure 6B), and then extrapolating the linear portion of the curve to zero absorption. The resultant indicated that the band gap was found to be 3.09 eV. Compared to the bulk ZnO, the optical band gap of the prepared NPs is smaller, which we believe to be due to the structural defects that arising during the sample synthesis. As it is well known, the point effects in ZnO introduce levels within the bandgap lead to the appearance of the wide deep level emission band covering the whole visible range. ZnO NPs exhibit a broad dominate luminescence band in the visible region due to the existence of several

different native point defects which including oxygen vacancy V_O , zinc vacancy V_{Zn} , oxygen interstitial O_i , zinc interstitial Zn_i , oxygen anti site, zinc anti sites, and clusters of native defects (V_O and Zn_i) (Choi et al., 2015). Defects are playing an important role on photodegradation because they will increase the materials photocatalytic activities within the visible light spectrum (Jucá et al., 2021).

The separation and migration rates of photogenerated electrons and holes were further investigated using a photoluminescence (PL) test. As shown in (Figure 6C), The PL spectra of pristine ZnO nanoparticle exhibited broad absorption bands at less than 250 nm, respectively, indicating that the electrons and holes can be easily recombined (Okab et al., 2023). Interestingly, a significant decrease in the PL intensity was detected related to the ZnO nanoparticle sample, corresponding to the synergistic. Furthermore, lower PL intensity was recorded by the ZnO nanoparticle sample. This observation confirms the ability of ZnO nanoparticle to facilitate the transfer efficiency of photoinduced electrons and holes and the recombination rate, which can develop the photodegradation activity (Lu et al., 2019). These findings agree with observations reported by (Yu et al., 2020; Fagier et al., 2021)

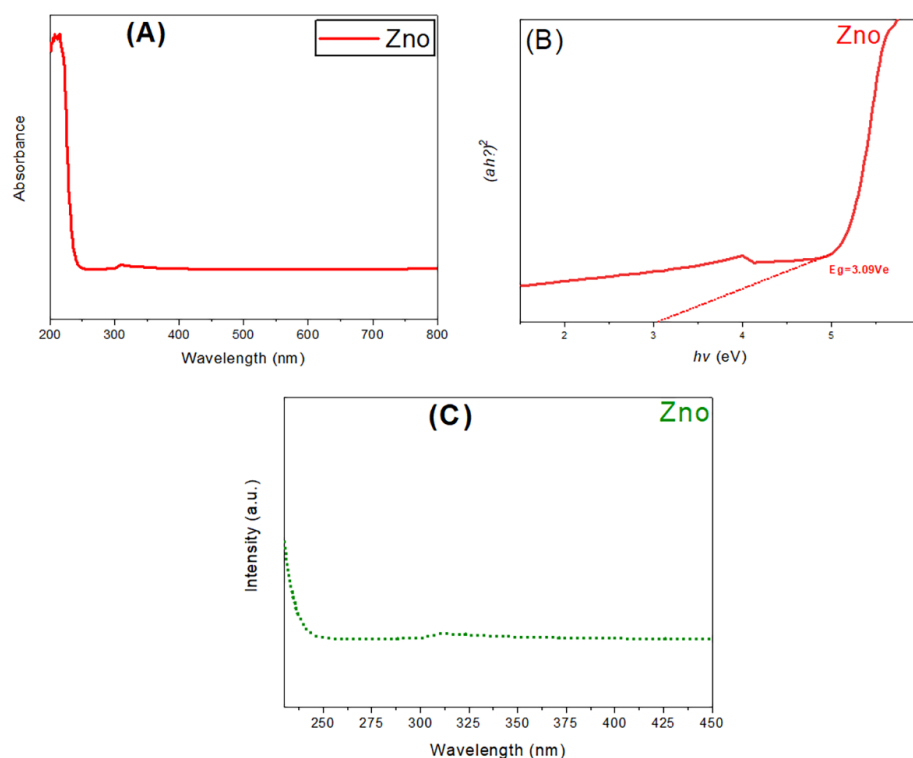


Figure 6. (A) The DRS spectra of ZnO (B) Band gap energy of ZnO, (C) PL spectra of ZnO.

Adsorption and photocatalytic activities

The adsorption and photodegradation activities of fabricated catalyst ZnO NPs towards sulfosulfuron herbicide are studied at different concentration of herbicides (10, 20, 40, and 80) mg/ Land constant pH (6.8), and dosage of g/L, and their results are illustrated in (Figure 7). Firstly, the solution was left for 30 min adsorption time followed by 150 min UV photocatalyst. According to the results, a slight degradation (less than 9%) was noticed in the darkness after 30 min. When the irradiation time began, though, the deterioration efficiency rose. Additionally, the findings demonstrate that the maximum degradation percentage results for 90 min irradiation was (82.08). The rate of photocatalytic degradation performance of a certain pollutant depends on significant factors that are governing the photocatalysis

processes factors can affect individually or/and together with the process (He et al., 2021).

Reusability of the catalyst

In practice, the photostability of the prepared catalyst is conducive to reducing water treatment costs and avoiding secondary pollution. To test the stability of the ZnO nanoparticle, the photocatalytic performance for sulfosulfuron degradation of ZnO samples while keeping other parameters constant from previous experiments. Each experiment lasted 90 min and the catalyst was collected and washed thoroughly with distilled water and then dried to be used in subsequent experiments, and their results were plotted in (Figure 8), it shows that there is reduction for sulfosulfuron efficiency from (82.08, and 58.97)% for ZnO, after four recycles.

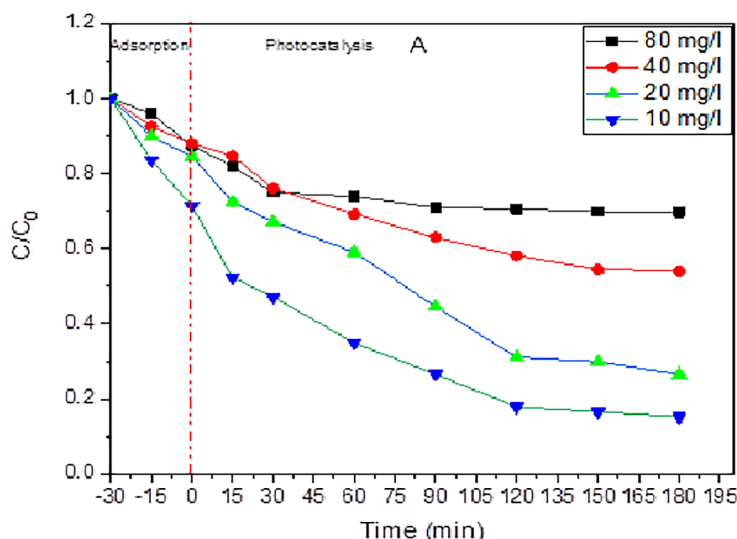


Figure 7. Photodegradation performance of 1g/L of ZnO with 10 mg/L of sulfosulfuron (pH of 6.8)

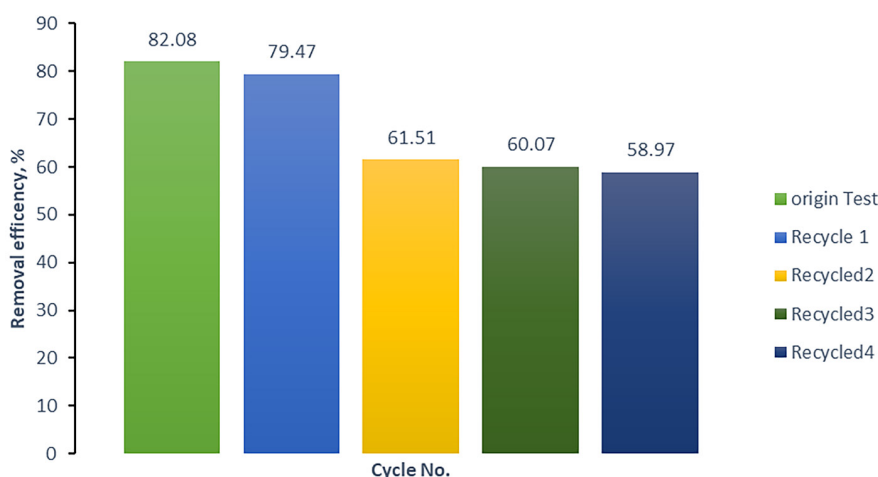


Figure 8. Sulfosulfuron herbicide degradation cycles at running time of 90 min

It indicated that photocatalyst possessed is stable enough for realistic environment remediation

Photodegradation kinetics

To quantitatively evaluate the photocatalytic activity of ZnO NPs, the first-order kinetics (Langmuir-Hinshelwood (L-H) kinetics model) (Ahmadpour et al., 2020) were implemented, and the results are illustrated in Table 1. The experimental data matched perfectly with pseudo-first-order kinetics (Equation 3) and yielded a high regression coefficient (R^2). Where C , C_0 , and k are the Sulfosulfuron concentrations at the attained time t , the initial Sulfosulfuron concentration, and the photodegradation rate constant, respectively. The evaluated k values were illustrated in (Figure 9) and (Table 1).

$$\ln \frac{C}{C_0} = -kt \quad (3)$$

where: the photodegradation rate constant (k), by plotting the $-\ln(C/C_0)$ vs. time (t).

Radical experiments and proposed mechanisms

Photocatalytic process is a reaction that depends on the catalyst and wavelength of light energy (photon), whether the light from sunlight or artificial light energy. Many researchers have described the mechanism of ZnO NPs photocatalytic

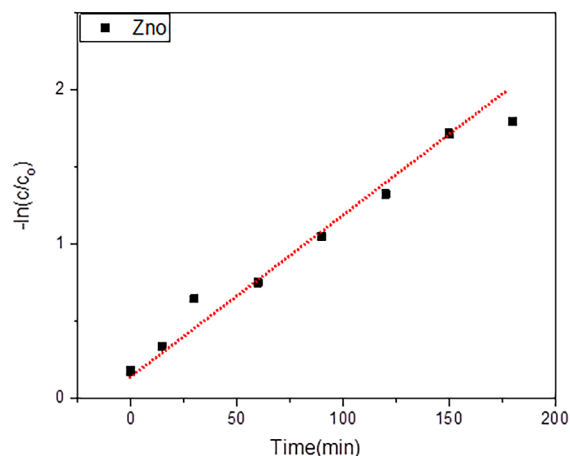


Figure 9. The first-order kinetic model

Table 1. The first-order kinetics results towards sulfosulfuron degradation

Photocatalyst	k/min	R^2
ZnO	0.00894	0.9889

reaction. Herrmann et al. (Herrmann et al., 1999) reported that ZnO NPs degrade organic pollutants, organic contaminants diffuse from the liquid phase to the surface of ZnO NPs, adsorption of the organic contaminants on the surface of ZnO NPs and then oxidation and reduction reactions take place in the adsorbed phase, desorption of the products and consequent removal of the products from the interface region (Ibhadon et al., 2013; Ong et al., 2018) explored the mechanism photocatalytic reaction of ZnO NPs, photocatalytic reactions are initiated when ZnO surface is exposed by a radiation of photonic energy ($h\nu$) equal to or greater than the ZnO band gap, photonic energy responds to excitation of the electrons and then produces electron-hole (e^-/h^+) pairs, one is a positively charged hole in the valence band (VB) and the other is a negatively charged electron in the conduction band (CB) (Equation 4), electron-hole pairs can transfer to the ZnO surface and be involved in redox reactions, positive holes (H^+) created in the valence band reacts with absorbed water and hydroxide ions to produce powerful hydroxyl radicals, hydroxyl radicals degrade the organic pollutants adsorbed on the surface of ZnO (Equations 5 and 6), conduction band electrons react with dissolved oxygen species to produce superoxide radical anions and then hydrogen peroxide (Equations 7–9). Hydrogen peroxide will then react with superoxide radicals to form hydroxy radicals which react with pollutants adsorbed on the surface of ZnO and then produce intermediate compounds that converted to green compounds such as CO_2 , H_2O , and mineral acids (Equations 10–13) depending on Equations 14–16.

Photocatalytic oxidation reaction depends on the generation and recombination of electrons and holes in the ZnO photocatalyst (Figure 10). Therefore, to ensure the photocatalytic process is accomplished, ZnO's quantum size, specific surface area of ZnO, and organic pollution concentration should be highly considered (Colmenares et al., 2009).

Numerous active groups, such as h^+ , $\bullet O_2^-$, and $\bullet OH$, are produced by the photocatalytic reaction and are essential to the photodegradation process. In this instance the ZnO nanoparticle, sulfosulfuron degradation process' primary active species were investigated by radical capture studies. Therefore, ethylenediaminetetraacetic acid (EDTA-2Na, $1 \text{ mmol} \cdot \text{L}^{-1}$) was utilized as a h^+ trapping agent, isopropanol (IPA, $1 \text{ mmol} \cdot \text{L}^{-1}$) as a $\bullet OH$ scavenging agent, and benzoquinone (BQ, $1 \text{ mmol} \cdot \text{L}^{-1}$) as an O_2^- scavenging agent (54). The

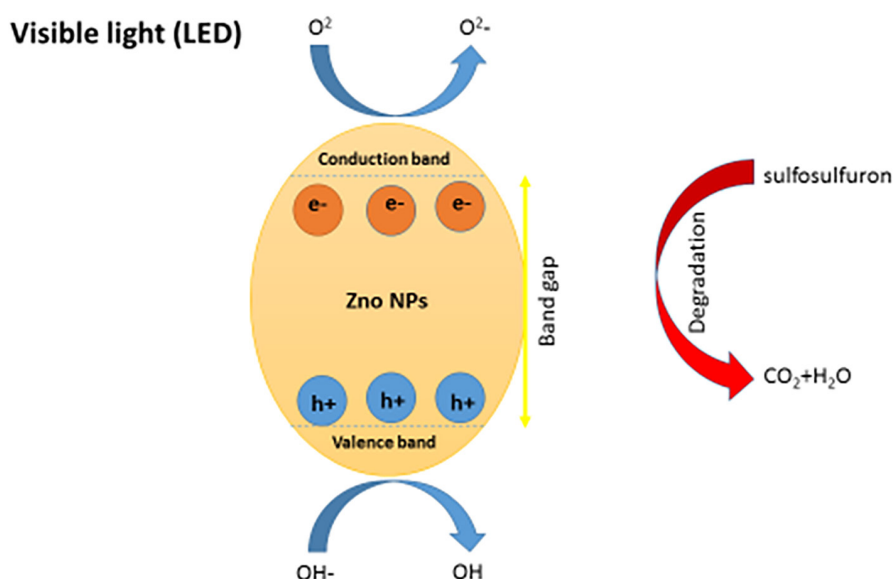
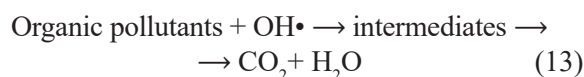
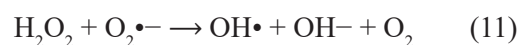
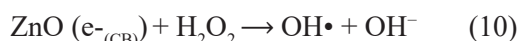
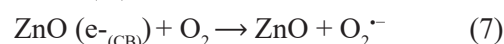
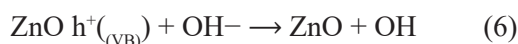
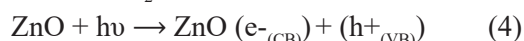


Figure 10. The schematic illustration of proposed mechanism for ZnO

photodegradation activity of sulfosulfuron was dramatically reduced (19.9%) upon the addition of the IPA scavenger, indicating that the primary reactive species is likely $\bullet\text{OH}$ (Figure 11). Moreover, adding BQ to the photoreaction resulted in a noticeably reduced sulfosulfuron removal efficiency (49.36%), suggesting that another significant oxidant is the $\bullet\text{O}_2^-$ radical. However, after being absorbed by the EDTA-2Na scavenger, the h^+ oxidant showed the lowest contribution, decreasing the elimination efficiency to 63.52%. As a result, the order of the oxidant's influence is as follows: $\text{OH} > \text{O}_2^- > \text{h}^+$.



$$\chi(A_m B_n C_l) = \sqrt[m+n+l]{\chi_A^m \chi_B^n \chi_C^l} \quad (14)$$

$$\text{VB} = \chi - E_e + 0.5E_g \quad (15)$$

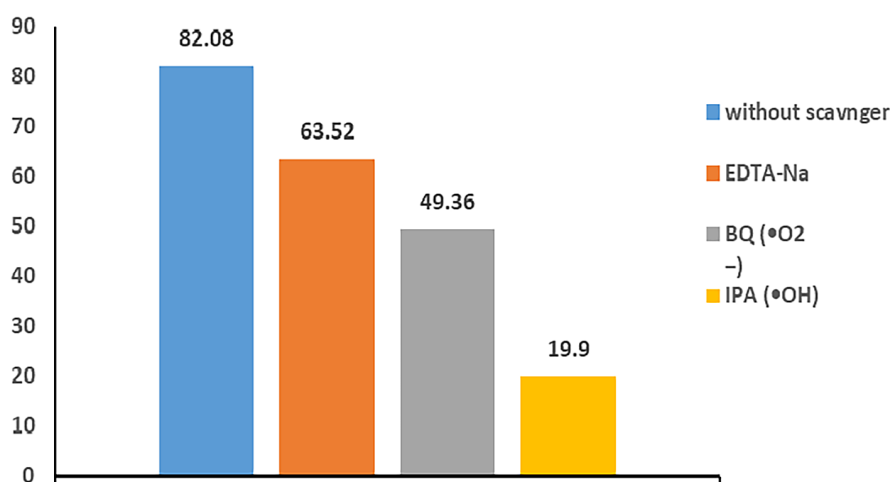


Figure 11. Reactive species scavenger reactions (sulfosulfuron concentration of 10 ppm, ZnO dosage of 1g/L, and illumination time = 90 min)

Table 2. Sulfosulfuron herbicide degradation performance of this work compared with previous studies

Green synthesis of zinc oxide	Catalyst dosage	Pollutant concentration	Light source	Time	Photo. efficiency (%)	References
Fresh lemon juice	100 mg/L	44.87mg/L	UV lamp	30 min	25%	(Patwa et al., 2021)
Root extract of <i>Scutellaria baicalensis</i>	0.016 mg	0.05 mg/ml	UV lamp	210 min	82%	(Chen et al., 2019)
Red dragon fruit	250 mg	10 mg/L	Visible light	120 min	98.82%	(Sorbiun et al., 2018)
Hagenia abyssinica leaf	40 mg	15 ppm	Sunlight irradiation	120 min	83.17%	(Zewde et al., 2022)
Olive leaves extract	1 g/L	10mg/L	Visible light	90 min	82.08%	This study

$$CB = VB - E_g \quad (16)$$

where: the VB of ZnO is 2.93 eV, while their CB is -0.155 eV; χ is semiconductor electronegativity (ZnO = 5.89 eV) (Pearson et al., 1988) and E_g is the free electrons energy (4.5 eV) towards hydrogen scale.

Comparison with previous studies

To assess the photodegradation activity of ZnO NPs, the photodegradation performance of this work was compared with other previous studies, and the results are summarized in Table 2. This compaction was assessed depending on some factors like the type of catalyst system, pollutant concentration, catalyst dosage, irradiation time, and removal efficiency. As a result, the ZnO NPs showed enhanced separation efficiency, developing a remarkable system for herbicides degradation with cost-effective technology.

CONCLUSIONS

Green synthesis ZnO nanoparticles were prepared using the extract of olive leaves and identified using FTIR, XRD- EDX, UV–Vis, PL, TEM and BET techniques, which confirmed the formation of NPs with an average size of 29.03 nm analysis. The results confirm the effectiveness of ZnO NPs to remove sulfosulfuron herbicide residues in batch mode reactor using visible light at intensity of 39.8 mW cm^{-2} , with a maximum removal percentage of 82.08% under optimum conditions of 10 mg/L of sulfosulfuron Herbicide concentration, and 90 min. In addition, the reaction followed a first-order kinetics model with R^2 more than 96%. The findings of this study show that ZnO NPs photocatalyst exhibits potential performance as an inexpensive and ecologically acceptable method for photocatalytic

degradation of herbicide, which provides a new insight into the elimination of herbicide removal from wastewater.

REFERENCES

1. Abbasian, R., Jafarizadeh-Malmiri, H. 2020. Green approach in gold, silver and selenium nanoparticles using coffee bean extract. *Open Agriculture*, 5(1), 761–767.
2. Abdelbaky, A.S., Abd El-Mageed, T.A., Babalghith, A.O., Selim, S., Mohamed, A.M. 2022. Green synthesis and characterization of ZnO nanoparticles using *Pelargonium odoratissimum* (L.) aqueous leaf extract and their antioxidant, antibacterial and anti-inflammatory activities. *Antioxidants*, 11(8), 1444.
3. Abdelbaky, A.S., Abd El-Mageed, T.A., Babalghith, A.O., Selim, S., Mohamed, A.M. 2022. Green synthesis and characterization of ZnO nanoparticles using *Pelargonium odoratissimum* (L.) aqueous leaf extract and their antioxidant, antibacterial and anti-inflammatory activities. *Antioxidants*, 11(8), 1444.
4. Abdulrazaq, H.A., Alwared, A.I. 2023. Bio-synthesis of TiO_2 using grape leaves extract and its application for photocatalytic degradation of ibuprofen from aqueous solution. *Environmental Technology*, 45(13), 2493–2505.
5. Abel, S., Tesfaye, J.L., Shanmugam, R., Dwarampudi, L.P., Lamessa, G., Nagaprasad, N., Benti, M., Krishnaraj, R. 2021. Research article green synthesis and characterizations of zinc oxide (ZnO) nanoparticles using aqueous leaf extracts of coffee (*Coffea arabica*) and its application in environmental toxicity reduction.
6. Ahmad, S., Munir, S., Zeb, N., Ullah, A., Khan, B., Ali, J., Bilal M., Omer M., Alamzeb M., Salman S.M., Ali, S. 2019. Green nanotechnology: A review on green synthesis of silver nanoparticles—An ecofriendly approach. *International journal of nanomedicine*, 5087–5107.
7. Al-Rbaihat, R., and Al-Marafi, M.N. 2023. Combined effect of silicon dioxide and titanium dioxide nanoparticles on concrete properties. *Journal of Ecological Engineering*, 24(12).

8. Alrubaie, E.A.A., Kadhim, R.E. 2019. Synthesis of ZnO nanoparticles from olive plant extract. *Plant Archives*, 19(2), 339–344.
9. Alwared A.A., Mohammed N.A., Al-Mosawi T.J., and Mohammed A.A. 2023. Solar-induced photocatalytic degradation of reactive red and turquoise dyes using a titanium oxide /xanthan gum composite, *Sustainability*, 15, 10815.
10. Andrade, P.H., Hureau, M., Mamede, A.S., Masiani, P., Legrand, A., Moissette, A. 2024. Long-lived charge-separated states in ZnS/Na-MOR zeolite upon trans-stilbene adsorption. *The Journal of Physical Chemistry C*, 128(11), 4639–4647.
11. Asemami, M., Anarjan, N. 2019. Green synthesis of copper oxide nanoparticles using *Juglans regia* leaf extract and assessment of their physico-chemical and biological properties. *Green Processing and Synthesis*, 8(1), 557–567.
12. Awwad, A.M., Albiss, B., Ahmad, A.L. 2014. Green synthesis, characterization and optical properties of zinc oxide nanosheets using *Olea europea* leaf extract. *Adv. Mater. Lett*, 5(9), 520–524.
13. Bhardwaj, A., Sharma, G., Gupta, S. 2020. Nanotechnology applications and synthesis of graphene as nanomaterial for nanoelectronics. *Nanomaterials and Environmental Biotechnology*, 251–269.
14. Chen, L., Batjikh, I., Hurh, J., Han, Y., Huo, Y., Ali, H., Jin Feng Li, Rupa E.J., Ahn J.C., Mathiyalagan R., Yang, D.C. 2019. Green synthesis of zinc oxide nanoparticles from root extract of *Scutellaria bicalensis* and its photocatalytic degradation activity using methylene blue. *Optik*, 184, 324–329.
15. Choi, S., Phillips, M.R., Aharonovich, I., Pornsawan, S., Cowie, B.C., Ton-That, C. 2015. Photo-physics of point defects in ZnO nanoparticles. *Advanced Optical Materials*, 3(6), 821–827.
16. Colmenares, J.C., Luque, R., Campelo, J.M., Colmenares, F., Karpiński, Z., Romero, A.A. 2009. Nanostructured photocatalysts and their applications in the photocatalytic transformation of lignocellulosic biomass: an overview. *Materials*, 2(4), 2228–2258.
17. Dash, D.K., Panik, R.K., Sahu, A.K., Tripathi, V. 2020. Role of nanobiotechnology in drug discovery, development and molecular diagnostic. In *Applications of nanobiotechnology*. IntechOpen.
18. Dhananjay, P., Abhilash, M.R., Shilpa, N., NK, H.K., Gowtham, H.G., Aiyaz, M., Singh, B.S., Malik, A., Akhtar, S., Murali, M. 2024. Solar irradiation driven catalytic dye degradation by novel biosynthesized zinc oxide nanoparticles (ZnO-NPs) from *Barleria mysorensis*: Kinetics, reusability and mineralization studies. *Journal of Molecular Structure*, 1303, 137549.
19. Fagier, M.A. 2021. Plant-mediated biosynthesis and photocatalysis activities of zinc oxide nanoparticles: a prospect towards dyes mineralization. *Journal of Nanotechnology*, 2021(1), 6629180.
20. Gnanasangeetha, D., Thambavani, D.S. 2013. Biogenic production of zinc oxide nanoparticles using *Acalypha indica*. *Journal of Chemical, Biological and Physical Sciences (JCBPS)*, 4(1), 238.
21. Hamouda, R., Elshamy, M. 2021. Using biosynthesized zinc oxide nanoparticles to alleviate the toxicity on banana parasitic-nematode. *Research*, 67.
22. Hashemi, S., Asrar, Z., Pourseyedi, S., Nadernejad, N. 2016. Green synthesis of ZnO nanoparticles by Olive (*Olea europaea*). *IET nanobiotechnology*, 10(6), 400–404.
23. He, Z., Yang, H., Su, J., Xia, Y., Fu, X., Wang, L., Kang, L. 2021. Construction of multifunctional dual Z-scheme composites with enhanced photocatalytic activities for degradation of ciprofloxacin. *Fuel*, 294, 120399.
24. Herrmann, J.M. 1999. Heterogeneous photocatalysis: fundamentals and applications to the removal of various types of aqueous pollutants. *Catalysis today*, 53(1), 115–129.
25. Ibhaddon, A.O., Fitzpatrick, P. 2013. Heterogeneous photocatalysis: recent advances and applications. *Catalysts*, 3(1), 189–218.
26. Jucá, A.C.S., Lopes, F.H.P., Silva-Júnior, H.V., Silva, L.K.R., Longo, E., Szancoski, J.C., Cavalcante, L. 2021. Structure, morphology features and photocatalytic properties of α -Ag₂WO₄ nanocrystals-modified Palygorskite clay. *J. Photocatal.*, 2(2), 114–129.
27. Lu, S., Li, J., Duan, F., Duan, L., Du, M., Chen, M. 2019. One-step preparation of Bi₄O₅Br_xI_{2-x} solid solution with superior photocatalytic performance for organic pollutants degradation under visible light. *Applied Surface Science*, 475, 577–586.
28. Mohammed N.A., Alwared A.I., Shakhir K.S., Sulaiman F.A. 2024. Synthesis, characterization of FeNi₃@SiO₂@CuS for enhance solar photocatalytic degradation of atrazine herbicides: Application of RSM, *Results in Surfaces and Interfaces*, 16, 100253.
29. Mohammed, N.A.A., Alwared, A.I., Salman, M.S. 2020. The decolorization of reactive yellow dye by advanced oxidation using continuous reactors. *Iraqi Journal of Chemical and Petroleum Engineering*, 21(2), 1–6.
30. Navarraa W., Saccoa O., Vaiano V., and Venditto V. 2023. Pesticides removal from wastewater using a pilot-scale photocatalytic reactor, *Chemical Engineering transactions* 98, 159–164.
31. Okab, A.A., Alwared, A.I. 2023. A dual S-scheme g-C₃N₄/Fe₃O₄/Bi₂WO₆/Bi₂S₃ heterojunction for improved photocatalytic decomposition of methylene blue: Proposed mechanism, and stability studies. *Materials Science in Semiconductor*

- Processing, 153, 107196.
32. Ong, C.B., Ng, L.Y., Mohammad, A.W. 2018. A review of ZnO nanoparticles as solar photocatalysts: Synthesis, mechanisms and applications. *Renewable and Sustainable Energy Reviews*, 81, 536–551.
 33. Paporisch, A., Laor, Y., Rubin, B., Eizenberg, H. 2020. Effect of repeated application of sulfonylurea herbicides on sulfosulfuron dissipation rate in soil. *Agronomy*, 10(11), 1724.
 34. Patil, M.P., Kim, G.D. 2017. Eco-friendly approach for nanoparticles synthesis and mechanism behind antibacterial activity of silver and anticancer activity of gold nanoparticles. *Applied microbiology and biotechnology*, 101, 79–92.
 35. Patwa R., Nabanita Saha N., Saha P. 2021. Green synthesis of zinc oxide nanoparticles, their characterization and utilization for photocatalytic removal of methylene blue, *Prayogik Raayan*. 2021 xx, 5(1), xx–xx.
 36. Patwa, R., Saha, N., Saha, P. 2021. Green synthesis of zinc oxide nanoparticles, their characterization and utilization for photocatalytic removal of methylene blue. *Pray. Rasayan*, 5.
 37. Pearson, R.G. 1988. Absolute electronegativity and hardness: application to inorganic chemistry. *Inorganic chemistry*, 27(4), 734–740.
 38. Pergal, M.V., Kodranov, I.D., Pergal, M.M., Dojčinović, B.P., Stanković, D.M., Petković, B.B., Manojlović, D.D. 2018. Assessment of degradation of sulfonylurea herbicides in water by chlorine dioxide. *Water, Air, & Soil Pollution*, 229, 1–11.
 39. Prasad, A.R., Ammal, P.R., Joseph, A. 2018. Effective photocatalytic removal of different dye stuffs using green synthesized zinc oxide nanogranelles. *Materials Research Bulletin*, 102, 116–121.
 40. Raafat, M., El-Sayed, A.S., El-Sayed, M.T. 2021. Biosynthesis and anti-mycotoxigenic activity of *Zingiber officinale* roscoe-derived metal nanoparticles. *Molecules*, 26(8), 2290.
 41. Sarli, S., Kalani, M.R., Moradi, A. 2020. A potent and safer anticancer and antibacterial taxus-based green synthesized silver nanoparticle. *International Journal of Nanomedicine*, 3791–3801.
 42. Schreyer, M., Guo, L., Thirunahari, S., Gao, F., Garland, M. 2014. Simultaneous determination of several crystal structures from powder mixtures: the combination of powder X-ray diffraction, band-target entropy minimization and Rietveld methods. *Journal of Applied Crystallography*, 47(2), 659–667.
 43. Sorbiun, M., Shayegan Mehr, E., Ramazani, A., Taghavi Fardood, S. 2018. Green synthesis of zinc oxide and copper oxide nanoparticles using aqueous extract of oak fruit hull (jaft) and comparing their photocatalytic degradation of basic violet 3. *International Journal of Environmental Research*, 12, 29–37.
 44. Sulaiman, F.A., and Alwared, A.I. 2022. Ability of response surface methodology to optimize photocatalytic degradation of amoxicillin from aqueous solutions using immobilized TiO₂/sand. *Journal of Ecological Engineering*, 23(5).
 45. Xu, Z., Wu, Y., Song, L., Chinnathambi, A., Alharbi, S.A., Fang, L. 2020. Anticarcinogenic effect of zinc oxide nanoparticles synthesized from *Rhizoma paradisi* saponins on Molt-4 leukemia cells. *Journal of King Saud University-Science*, 32(3), 1865–1871.
 46. Yu, J., Jaroniec, M., Jiang, C. (Eds.). 2020. Surface science of photocatalysis. Academic Press.
 47. Zewde, D., Geremew, B. 2022. Biosynthesis of ZnO nanoparticles using *Hagenia abyssinica* leaf extracts; their photocatalytic and antibacterial activities. *Environmental pollutants and bioavailability*, 34(1), 224–235.
 48. Zhang, X., Wang, X., Meng, J., Liu, Y., Ren, M., Guo, Y., Yang, Y. 2021. Robust Z-scheme g-C₃N₄/WO₃ heterojunction photocatalysts with morphology control of WO₃ for efficient degradation of phenolic pollutants. *Separation and Purification Technology*, 255, 117693.